Argonautes ALG-3 and ALG-4 are required for spermatogenesis-specific 26G-RNAs and thermotolerant sperm in *Caenorhabditis elegans*

Colin C. Conine[a], Pedro J. Batista[a,b], Weifeng Gu[a], Julie M. Claycomb[a,c], Daniel A. Chaves[a,d], Masaki Shirayama[a], and Craig C. Mello[a,c,1]

[c]The Howard Hughes Medical Institute, and [a]Program in Molecular Medicine, University of Massachusetts Medical School, Worcester, MA 01606; [b]Gulbenkian PhD Programme in Biomedicine, Rua da Quinta Grande, 6, 2780-156 Oeiras, Portugal; and [d]Instituto de Medicina Molecular, Faculdade de Medicina, Universidade de Lisboa, Avenida Professor Egas Moniz, 1649-028 Lisbon, Portugal

Edited* by Gary Ruvkun, Massachusetts General Hospital, Boston, MA, and approved December 30, 2009 (received for review October 14, 2009)

Gametogenesis is a thermosensitive process in numerous metazoans, ranging from worms to man. In *Caenorhabditis elegans*, a variety of RNA-binding proteins that associate with germ-line nuage (P granules), including the Piwi-clade argonaute PRG-1, have been implicated in maintaining fertility at elevated temperature. Here we describe the role of two AGO-class paralogs, *alg-3* (T22B3.2) and *alg-4* (ZK757.3), in promoting thermotolerant male fertility. A rescuing GFP::*alg-3* transgene is localized to P granules beginning at the late pachytene stage of male gametogenesis. *alg-3/4* double mutants lack a subgroup of small RNAs, the 26G-RNAs which target and appear to down-regulate numerous spermatogenesis-expressed mRNAs. These findings add to a growing number of AGO pathways required for thermotolerant fertility in *C. elegans* and support a model in which AGOs and their small RNA cofactors function to promote robustness in gene-expression networks.

gene expression | RNAi | germline | P granules | spermiogenesis

Argonaute (AGO) proteins have been implicated in gene silencing in fungi, plants, protozoans, and metazoans including humans. They are ~100-kDa highly basic proteins that are characterized by the presence of PAZ and PIWI domains and by their association with small RNA species (reviewed in ref. 1). Argonautes can be classified into three clades (2): (*i*) the AGO clade, which includes the human AGOs1-4, the *Caenorhabditis elegans* miRNA effectors ALG1/2, and all of the *Arabidopsis thaliana* AGOs; (*ii*) the Piwi clade, which more closely resembles *Drosophila* Piwi and includes the *C. elegans* piRNA AGO PRG-1; and (*iii*) an expanded family of worm-specific AGOs (WAGOs) that, with a few exceptions, lack residues in the PIWI domain thought to be necessary for slicer endonuclease activity.

In *C. elegans*, null mutations are available for the entire family of over 24 AGO genes (3), and at least five different combinations of these mutants result in lethal or sterile phenotypes. *alg-1/2* mutants display heterochronic defects and lethality that arise from loss of miRNA-mediated regulation of developmentally important transcripts (4). *csr-1* mutants have severe chromosome segregation defects that result in embryonic lethality (3, 5), and *prg-1* mutants have severe defects in the development of the germline (6–8). In addition, the simultaneous deletion of 12 WAGOs leads to a temperature-sensitive sterile phenotype, where mutants are viable and fertile at 20 °C but sterile at 25 °C (9).

Here we describe two paralogous AGO-clade family members, *alg-3* and *alg-4*, that are together critical for sperm development and function. Single mutants have only a minor reduction in brood size, but double *alg-3/4* mutants exhibit drastically reduced brood sizes at elevated temperatures. We show that a rescuing GFP::ALG-3 protein is expressed in germ cells undergoing spermatogenesis and that, even though both male and hermaphrodite *alg-3/4* mutants produce near wild-type numbers of spermatids, these spermatids exhibit severe defects in the activation process called spermiogenesis that converts spermatids into motile ameboid sperm.

A class of 26nt small RNAs called the 26G-RNAs were first identified in deep-sequencing datasets in *C. elegans* as part of the previously described Dicer-ribonuclease-dependent endogenous small RNA pathway, called the ERI pathway, and a subset of these were noted to be enriched for spermatogenesis-expressed mRNA targets (10–13). Here we show that, like their targets, a subset of 26G-RNAs are specifically expressed in the male germline and that their accumulation depends on the ALG-3/4 AGOs. Our findings suggest that ALG-3/4 function directly or indirectly in concert with 26G-RNAs and with other components of the ERI pathway to negatively regulate the steady-state levels of their target transcripts. Together with findings described by Vasale et al. (14), our study supports a two-step AGO model in which an initial round of AGO/26G-RNA-mediated targeting triggers the production of secondary small RNAs (called 22G-RNAs) that engage a distinct argonautes to amplify the silencing signal.

Our findings add to a growing number of argonaute-mediated pathways that promote robust-thermotolerant fertility in *C. elegans*. Argonautes acquire specificity through their RNA cofactors, and thus in principle have virtually unlimited capacity for sequence-specific gene regulation. We propose that AGO systems may use their versatile and highly adaptable nature to promote robustness in gene expression networks.

Results

Mutations in the *alg-3/4* AGOs Result in Male-Associated Temperature-Sensitive Sterility. The AGO-clade argonautes *alg-3* and *alg*-4 exhibit 96% sequence identity at the amino acid level (Fig. S1), as well as nucleotide homology that extends into the 5′ and 3′ noncoding regions. Consistent with the idea that *alg-3* and *alg-4* are recently duplicated genes, our genetic tests suggested that they retain partially overlapping functions. When compared to wild type, the *alg-3(tm1155)* single mutant exhibited a 2-fold decrease in brood size at 20 °C, and a 2.5- fold decrease at 25 °C (Fig. 1*A*). Similarly, *alg-4(ok1041)* and *alg-4(tm1184)* displayed a 2-fold decrease in brood size at 20 °C, and 3-fold decrease at 25 °C

Author contributions: C.C.C., P.J.B., and J.M.C. designed research; C.C.C., P.J.B., J.M.C., and D.A.C. performed research; C.C.C., P.J.B., and M.S. contributed new reagents/analytic tools; C.C.C., P.J.B., and W.G. analyzed data; and C.C.C., P.J.B., and C.C.M. wrote the paper.

The authors declare no conflict of interest.

*This Direct Submission article had a prearranged editor.

Freely available online through the PNAS open access option.

Data deposition: The sequence reported in this paper has been deposited in the National Center for Biotechnology Information Gene Expression Omnibus (accession no. GSE18731).

[1]To whom correspondence should be addressed. E-mail: craig.mello@umassmed.edu.

This article contains supporting information online at www.pnas.org/cgi/content/full/0911685107/DCSupplemental.

(Fig. 1*A*). However, when *alg-3(tm1155)* was combined with *alg-4 (ok1041)*, the resulting double mutants exhibited a 3-fold decrease in brood size at 20 °C and complete sterility at 25 °C (Fig. 1*A*).

To determine whether the sterility of *alg-3; alg-4* (*alg-3/4)* double-mutant hermaphrodites reflects a general deficit in gametogenesis or, alternatively, is specific to either spermatogenesis or oogenesis, we created obligate male/female populations. To do this we used a *fog-2* mutant that results in the feminization of hermaphrodites (15). In the following crosses, all of the individuals are *fog-2* mutants, and for simplicity we refer to animals with wild-type *alg-3* and *alg-4* activities as "*fog-2* males" or "*fog-2* females" and to *alg-3*; *alg-4* double mutants as "*alg-3/4* males" or "*alg-3/4* females." When mated to either *fog-2* females or *alg-3/4* females, *alg-3/4* males sired half as many progeny as *fog-2* males at 20 °C, and were almost completely sterile at 25 °C (Fig. 1*B*). In contrast, *alg-3/4* females were only slightly less fertile than *fog-2* females when mated to *fog-2* males. These data indicate that the sterility of *alg-3/4* mutants arises primarily from defects specific to the male germline.

To determine the temperature-sensitive period for *alg-3/4*-associated sterility, hermaphrodites reared at either 20 °C or 25 °C were shifted to the converse temperature (either up to 25 °C or down to 20 °C) as L2, L3, or L4 larva, or as gravid adults (16). When shifted up from 20 °C to 25 °C at or before the L4 stage, *alg-3/4* hermaphrodites were completely sterile (Fig. S2). Conversely, fertility was partially restored when *alg-3/4* animals were shifted down from 25 °C to 20 °C anytime before the L4 stage (Fig. S2). Fertility could not, however, be restored by shifting adults reared at 25 °C down to 20 °C, demonstrating that the temperature-sensitive sterility is at that point irreversible. Taken together, these data place the male-fertility defect at the L4 stage, coincident with the timing of spermatogenesis.

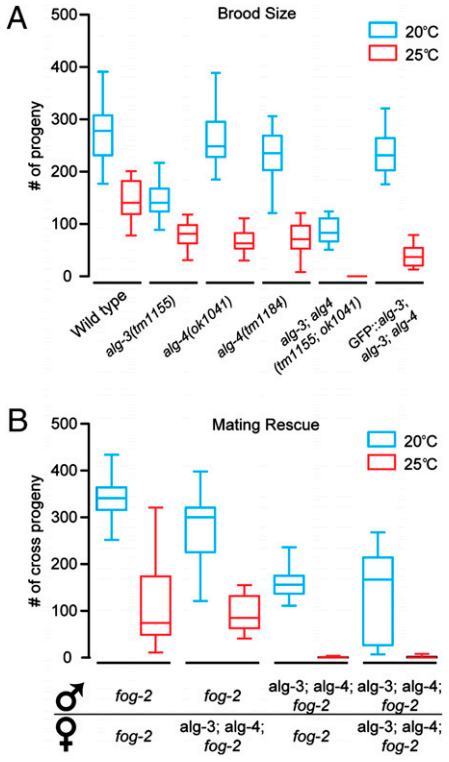

Fig. 1. *alg-3/4* mutants exhibit temperature-sensitive sterility associated with the male germline. (*A* and *B*) Box-and-whiskers plots of brood size in wild-type and mutant strains as indicated for ($n > 20$) animals cultured at 20 °C (blue) and 25 °C (red). In these and all subsequent box-and-whisker plots, the top and bottom ends of each box represent the 75th and 25th percentile, respectively; the line in the middle represents the median value; and the extended lines illustrate the range (highest and lowest value). The temperature of cultivation is indicated by color. (*A*) Self-crosses; (*B*) crosses between *fog-2* (wild-type) and *alg-3/4;fog-2* (mutant) worms.

ALG-3 Is Expressed in the Region of the Germline Undergoing Spermatogenesis. To examine the localization of ALG-3, we generated a full-length, N-terminally tagged GFP::*alg-3* transgenic line under the control of the *alg-3* promoter and 3′UTR. This transgenic line rescues *alg-3*; *alg-4* brood size to a level near the single *alg-4 (ok1041)* mutant (Fig. 1*A*). In GFP::*alg-3* hermaphrodites and males, GFP expression was observed in the proximal germline beginning at the L4 stage (Fig. 2*A* and Fig. S3*A*), coincident with the onset of spermatogenesis. In adult hermaphrodites, after the switch to oogenesis, GFP::ALG-3 expression was restricted to the spermatheca. Within the spermatheca, in hermaphrodites and testis in males, GFP::ALG-3 was localized within residual bodies, which are enucleate cytoplasts produced by the budding off of mature spermatids at the end of meiosis II. Little if any GFP::ALG-3 could be detected in mature spermatids (Fig. 2 *B* and *C* and Fig. S3*B*). As expected, the proximal expression of GFP::ALG-3 continued through adulthood in males (Fig. 2*C* and Fig. S3*C*). Within the developing spermatocytes, GFP::ALG-3 was first apparent in the postpachytene germline before the point where chromosomes appear to aggregate into a single mass (Fig. 2*A*) (17). GFP signal was localized throughout the cytoplasm and enriched at perinuclear foci coincident with P granules based on colocalization with RFP::PGL-1 (Fig. 2*B*) (18). The developmental expression profile of *alg-3* mRNA mirrored that of GFP::ALG-3 protein expression and was enriched in male-enriched populations and depleted in female populations (Fig. S3*D*).

***alg-3/4* Double Mutants Exhibit Defects in Spermatogenesis and Spermiogenesis.** To investigate the underlying cause of the *alg-3/4* male germline-associated sterile phenotype, we examined the development and numbers of *alg-3/4* spermatids in more detail. Relative to *fog-2* males, *alg-3/4* males produced approximately

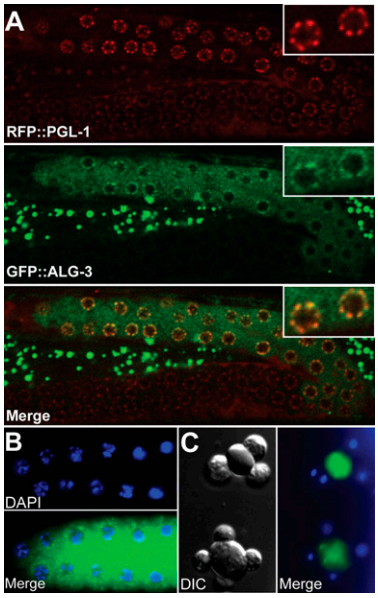

Fig. 2. GFP::ALG-3 is expressed during spermatogenesis. (*A–C*) Micrographs of ALG-3::GFP (green), nuclear staining/DAPI (blue), and PGL-1::RFP (red). (*A*) Confocal images in a young adult hermaphrodite. (*B*) Onset of expression in the proximal region of a male gonad. (*C*) Nomarski and fluorescence images of spermatids attached to residual bodies.

wild-type numbers of spermatids at 20 °C, and at 25 °C produced 29% fewer than wild type (Fig. 3*A*). This reduction in mature spermatids at the nonpermissive temperature was correlated with the persistence of abnormal secondary (2°) spermatocytes into adulthood (Fig. S4). These 2° spermatocytes appeared to be arrested as large dinucleate masses or as spermatids that fail to bud from the residual body. Chromosome bridging was observed in 20% of abnormal secondary spermatocytes in both males and hermaphrodites, indicating possible segregation defects during meiosis (Fig. S4). Hence, a reduction in the number of spermatids and defects in meiotic cell division could contribute to the fully sterile phenotype of *alg-3/4* double mutants at the nonpermissive temperature. However, many apparently normal spermatids are produced in *alg-3/4* mutants at both the permissive and nonpermissive temperatures. We therefore wondered whether a defect in spermiogenesis also existed. During spermiogenesis, activated spermatids form spikes that protrude from the cell and subsequently rearrange into a single pseudopod (19). In vivo, male spermatids are activated upon ejaculation, while hermaphrodite spermatids are activated when an oocyte enters the spermetheca (20). In vitro, spermiogenesis can be induced by treating isolated spermatids with pronase (19). Relative to *fog-2*, 20% fewer *alg-3/4* spermatids isolated from males were activated by pronase, as indicated by the formation of spike-like structures at permissive temperature (Fig. 3*B*). Strikingly, only 10% of activated *alg-3/4* spermatids progressed to form pseudopods, compared to 57% of activated wild-type spermatids. Instead, the *alg-3/4* spermatids accumulated many abnormal, long spike-like structures and failed to become motile (Fig. 3*C*). At nonpermissive temperature, this defect increased, as less than 2% of spermatids examined formed pseudopods compared to 54% for wild-type (Fig. 4*B*).

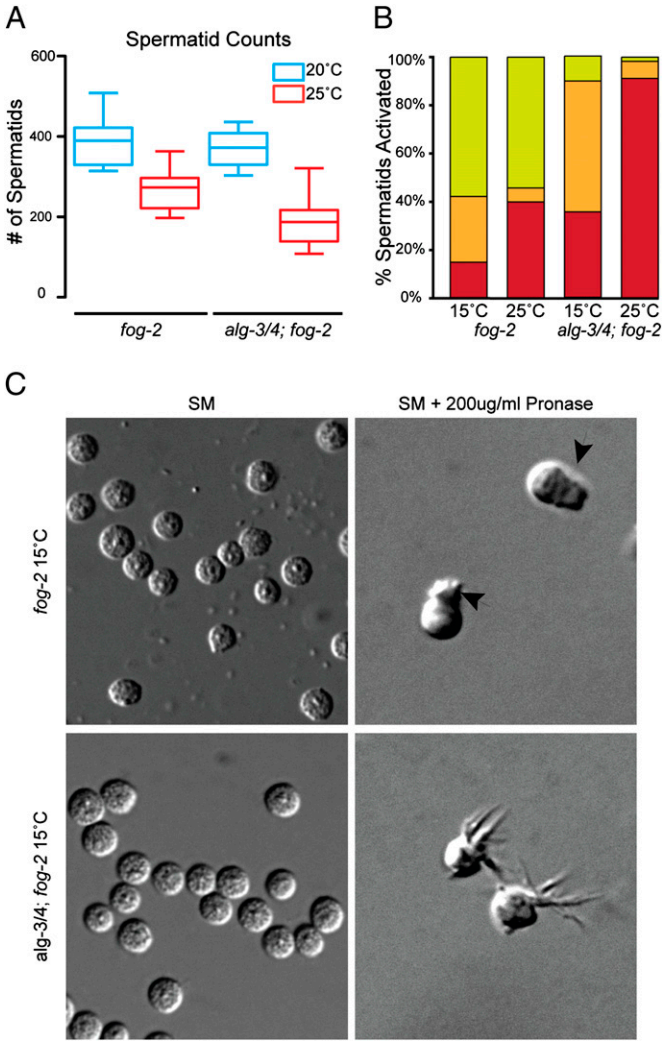

Fig. 3. *alg-3/4* mutants exhibit defects in sperm activation. (*A*) Box-and-whisker plots of spermatid counts performed on ($n > 20$) wild-type (*fog-2*) and *alg-3/4;fog-2* animals (as indicated) cultured at 20 °C (blue) or 25 °C (red). (*B*) Graphic depiction of spermatid activation, illustrating the percent of spermatids with pseudopods (green), spikes (orange), or unactivated (red) ($n > 200$). (*C*) Nomarski images of wild-type (*fog-2*) and *alg-3/4;fog-2* spermatids before (*Left*) and after (*Right*) activation. Black arrowheads denote pseudopods.

A Class of Sperm-Specific 26G-RNAs Requires *alg-3* and *alg-4*. Small RNAs that engage specific AGOs are often depleted in the corresponding AGO mutant backgrounds (4, 6, 9). Therefore, we used Illumina deep sequencing to identify small RNA species that were depleted in the *alg-3/4* mutant background. Small RNAs were isolated from male-enriched *fog-2* and *alg-3/4* populations, as well as mature sperm isolated from *fem-3* hermaphrodites, which overproduce sperm. To ensure that both 5′ monophosphorylated and 5′ triphosphorylated small RNAs would be amenable to ligation, samples were pretreated with tobacco acid pyrophosphatase before cloning (9). In both the wild-type and *alg-3/4* datasets, the majority of small RNAs were found within a large peak in the 21 to 23nt size range, corresponding to microRNAs, 21U-RNAs, and 22G-RNAs (Fig. 4*A*) (6, 9, 10). Strikingly, a second, much smaller peak at 26nt was observed in the wild-type dataset but was completely absent in the *alg-3/4* dataset (Fig. 4*A*). A strong bias for guanine at the 5′ residue of the 26 nt RNA species (86% of the 67,206 reads in wild type) allowed us to identify these small RNAs as 26G-RNAs (10). Interestingly, *alg-3/4*-dependent 26G-RNAs exhibited a strikingly lower abundance in mature sperm when compared to the whole-male samples. Overall, 26G-RNAs were 7-fold less abundant in mature sperm, a finding consistent with the expression pattern of GFP::ALG-3 protein, which was detected in developing spermatocytes but not in spermatids.

Most male-enriched 26G-RNAs were antisense to the expressed regions of endogenous *C. elegans* genes (Fig. 4*B* and ref. 10). All together, 3,191 genes were targeted by 26G-RNAs found in our wild-type samples, including 733 genes whose mRNAs were previously identified as enriched during spermatogenesis (21). In contrast, only 1,093 genes (279 spermatogenesis-enriched) were targeted by 26G-RNAs in the *alg-3/4* mutant data sets (Tables S1 and S2). To create a more stringently defined set of 26G-targeted genes, we applied a cutoff that included only genes targeted by at least 10 26G reads per million total reads. This higher-confidence set included 400 genes targeted by 26G-RNAs in wild-type, while only 4 genes were targeted in *alg-3/4* mutants. Among the 400 stringently-defined 26G-RNA targets, 397 genes (> 98%) were at least 2-fold depleted of 26G-RNAs in *alg-3/4* mutants (Fig. 4*E* and Table S3). The majority of 26G-RNAs that were not dependent on *alg-3/4* activity were dependent on *ergo-1*, which encodes an AGO required for a subset of 26G-RNAs that are abundantly expressed in embryos (14).

We used microarray analysis of young-adult RNA preparations to ask if the mRNAs targeted by 26G-RNAs were misregulated in *alg-3/4* mutants (Fig. 4*C*). Strikingly, we found that 109 of the 397 most stringently defined targets were up-regulated by 2-fold or more in the *alg-3/4* mutants (Figs 4*C* and 4*E*, and Table S4). Real-time quantitative RT-PCR (RT-qPCR) analysis of seven *alg*-3/4 26G-RNA targets confirmed the microarray analysis: Five targets that were up-regulated in the microarrays were also up-regulated by RT-qPCR, and two targets that were unchanged in the microarray analysis were also unchanged in the

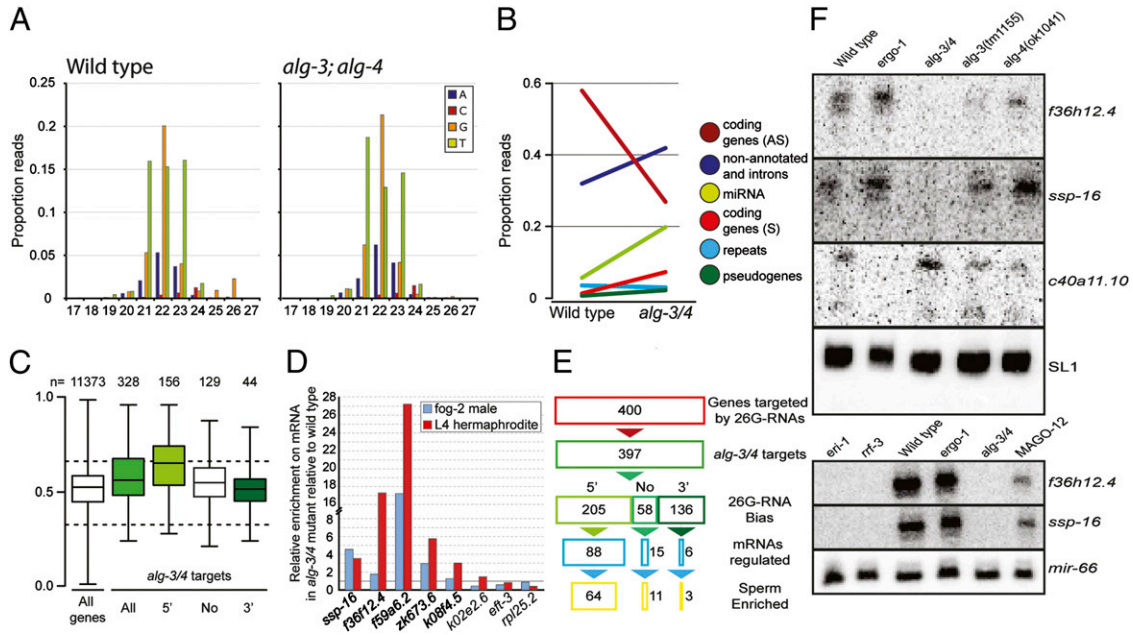

Fig. 4. Analysis of 26G-RNA expression and targeting. (*A*) Length and first-nucleotide distribution of deep-sequencing reads from wild-type (*fog-2*) (Left), and *alg-3/4; fog-2* (*Right*). (*B*) Two-point plots comparing the relative proportions of various small RNA classes (as indicated by color) in wild-type (*fog-2*) (*Left*) and *alg-3/4; fog-2* mutants (*Right*) for 26nt long reads. (*C*) Box-and-whisker plots depicting relative mRNA levels in microarray assays on *alg-3/4* (mutant) and N2 (wild-type) populations. Here and in Fig. 5, the *y* axis represents the relative mRNA levels [measured as (*alg-3/4* mutant value divided by [wild-type plus *alg-3/4* mutant values]) for any given locus]. Dotted lines indicate the values corresponding to 2-fold enrichment (a value of 0.66) or depletion (a value of 0.33). (*D*) RT-qPCR measurement of target mRNAs up-regulated (bold type) or not regulated (regular type) based on microarray analysis. *k02e2.6* is an *ergo-1*-dependent 26G-RNA target. (*E*) Schematic representation of 26G-RNA targets defined using using a cutoff of 10 reads per million. (*F*) Northern blot analysis of small RNAs in wild-type and various mutant backgrounds as indicated. SL1 and *mir-66* are loading controls.

RT-qPCR assay (Fig. 4*D*). As expected, an ERGO-1-dependent 26G-RNA target was not up-regulated in *alg-3/4* mutants.

ALG-3/4-dependent 26G-RNAs were not distributed randomly along their targets. Instead we noted a marked bias for accumulation at the termini of the transcripts (Fig. S5). Approximately half of the targets exhibited a bias for 5′ accumulation of 26G-RNAs, while 34% exhibited a 3′ bias (Fig. 4*E*). Strikingly, the mRNA levels of genes targeted by 26G-RNAs with a bias for 5′ accumulation showed higher levels of up-regulation: 85% of the 109 targets up-regulated in the *alg-3/4* mutants based on microarray analysis exhibited a 5′ bias for 26G-RNA accumulation. In contrast, only 5.5% of up-regulated targets exhibited a 3′ bias. The remaining 9.5% exhibited no bias (Fig. 4*E*).

Finally, we used Northern blot analysis to examine the expression of representative 26G-RNA species. We found that 26G-RNAs targeting *f36h12.4* and *ssp-16* were not detectable in *alg-3/4* mutants when compared to wild type, but were unaltered in *ergo-1* mutants (Fig. 4*F*). In *alg-3(tm1155)* and *alg-4(ok1041)* single mutants, these 26G-RNAs were only partially reduced (Fig. 4*F*). Conversely, a probe designed to detect 26G-RNAs from an *ergo-1*-dependent 26G-RNA target (14) *c40a11.10* revealed strong depletion in the *ergo-1* mutants, but showed no change in abundance in *alg-3/4* mutants. Spermatogenesis-expressed 26G-RNAs were also missing in *rrf-3 and eri-1,* supporting the placement of these small RNAs in the ERI pathway. Interestingly, the presence of these 26G-RNAs were only partially reduced in, a multiple mutant lacking all 12 WAGO genes (MAGO-12). These findings are consistent with the idea that spermatogenesis-specific 26G-RNAs depend on *alg-3* and *alg-4*, while 26G-RNAs expressed at other stages depend on *ergo-1* (Fig. 4*F* and ref. 14).

***wago-1*- and *alg-3/4*-Dependent 22G-RNAs Are Expressed in Mature Spermatids.** Two recent studies identified distinct 22G-RNA populations that interact with the argonautes WAGO-1 and CSR-1 (5, 9), but did not explore 22G-RNA expression in sperm. We found that 22G-RNAs represented ~70% of all small RNAs cloned from sperm (Fig. 5*A*), a proportion comparable to that observed in small RNAs recovered from gravid adult samples (9). Among the 397 targets that exhibited depletion of 26G-RNAs in *alg-3/4* mutants, 185 also exhibited a twofold or greater depletion in 22G-RNAs (Fig. 5*C* and Table S5). In contrast to the expression pattern of 26G-RNAs, which were less abundant in mature sperm samples than in male-enriched samples, the overall level of 22G-RNAs that target *alg-3/4* 26G-RNA targets was not changed in the sperm sample relative to the male-enriched sample.

Because WAGO proteins interact with 22G-RNAs (9), we asked whether WAGOs were present in and required for spermatid function. Consistent with this possibility, MAGO-12 mutants exhibit a temperature-sensitive sterile phenotype (9). We found that the sterility of MAGO12 hermaphrodites could be partially rescued by mating with wild-type males: Crosses with wild-type males at 25 °C produced an average brood of 29.8 progeny, compared with an average brood of 5.7 for self-mated hermaphrodites. Furthermore, we found that a GFP::WAGO-1 translational fusion was expressed throughout the germline and, unlike GFP::ALG-3, was also present in mature spermatids (Fig. 5*B*).

Discussion

Argonautes and their associated small RNAs function in gametogenesis in all metazoans. The best-studied examples are Piwi-clade AGOs, which function in the suppression of transposon activity in mammals, insects (reviewed in ref. 22), and nematodes (6, 7). Here, we have shown that two AGO-class paralogs, *alg-3* and *alg-4,* function during male gametogenesis to promote fertility at elevated temperatures (thermotolerance). Interestingly, these AGOs are required for a species of 26nt RNA called (26G-RNAs) that are antisense to hundreds of spermatogensis-enriched mRNAs (rather

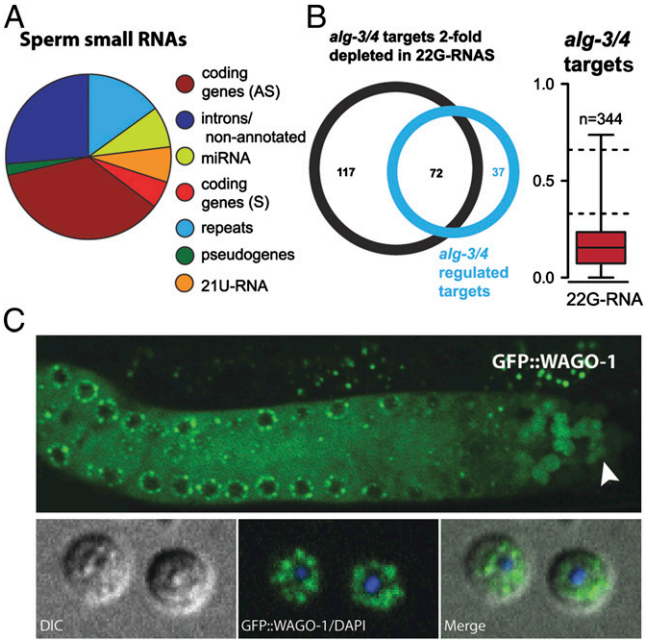

Fig. 5. Analysis of Small RNA pathways in mature sperm. (*A*) Pie chart representing the distribution of different classes of small RNA present in isolated spermatids. The 26nt RNAs represent less than 2% of the total small RNA reads. (*B*) *alg-3/4* targets are also 22G-RNA targets. The Venn diagram shows intersection between regulated *alg-3/4* targets (based on microarray) and targets that are depleted 2-fold or greater of 22G-RNAs. The box-and-whisker diagram shows depletion of 22G-RNAs relative to wild-type on *alg-3/4* targets. *y* axis represents the relative proportion of reads (measure as *alg-3/4* mutant value divided by wild type value plus *alg-3/4* mutant value). (*C*) GFP::WAGO-1 expression in an adult male (*upper panel*). Spermatids are marked with a white arrow head. GFP::WAGO-1 expression in individual spermatids, also stained with DAPI (blue, *lower panel*).

than to transposons or repetitive elements). Moreover, many of the genes targeted appear to be down-regulated in response.

A subset of 26G-RNAs are expressed during embryogenesis and depend on a distinct argonaute, ERGO-1 (14, 23). Vasale et al. (14), propose a model for ERGO-1-dependent 26G-RNAs that involves two rounds of RNA templated small RNA production and mRNA targeting. In this two-step model, ERGO-1 interacts directly with 26G-RNAs produced by the ERI-complex-associated RNA dependent RNA polymerase (RdRP), RRF-3. The resulting ERGO-1/26G-RNAs then recognize mRNA targets. However, rather than directly down-regulating these targets, the initial targeting recruits a second RdRP (RRF-1 and/or EGO-1), which then produces 22G-RNAs that are loaded onto WAGO-class argonautes to mediate silencing (14). Finally, whereas ERGO-1 and its associated 26G-RNAs are abundant during embryogenesis, the corresponding 22G-RNAs on the ERGO-1 targets are abundant throughout later larval development and into adulthood.

Several of our findings are consistent with a similar two-step model for ALG-3/4-dependent 26G-RNAs (Fig. 6*A*). First, ALG-3 expression is required for and coincides with expression of the spermatogenesis-expressed 26G-RNAs. Second, as was the case for ERGO-1, ALG-3/4 are also required for the expression of 22G-RNAs on their targets. Finally, whereas both ALG-3 and 26G-RNAs are depleted in mature sperm, WAGO-1 and the ALG-3/4-dependent 22G-RNAs remain abundant in mature sperm. Taken together, these findings support a model in which ALG-3/4 are loaded with 26G-RNAs produced by the ERI-Dicer-complex during spermatogenesis. These in turn, may induce the recruitment of a second RdRP to produce 22G-RNAs that persist as WAGO-1 complexes in mature sperm. This two-step AGO system could function to control the levels of mRNAs important for sperm function, perhaps by down-regulating in mature sperm a set of transcripts expressed during spermatogenesis (Fig. 6*B*). Persistence of WAGO-1 22G-RNA complexes in mature sperm may also provide a mechanism for the inheritance of epigenetic silencing signals important for fertility.

AGOs, Temperature-Sensitive Sterility, and P Granules. Wild-type animals exhibit sterility when cultured just 2 °C above the optimum growth range of 20 to 25 °C (24), suggesting that one or more aspect of gametogenesis involves an inherently temperature-sensitive process. In addition to *the alg-3*; *alg-4* mutants and the 12-fold WAGO mutants discussed above, mutations in the Piwi-related AGO, *prg-1,* cause temperature-dependent sterility. Mutations in a fourth AGO, *csr-1,* cause nonconditional sterility and chromosome segregation defects.

Interestingly, ALG-3, WAGO-1, PRG-1, and CSR-1 all localize to germline nuage structures called P granules, and *csr-1* mutants exhibit dramatic mislocalization of the P granules away from the periphery of germ-cell nuclei (5, 6, 9). Furthermore, mutations in other P-granule components that cause defects in the localization of the P granules, including *pgl-1* and *glh-1* (18, 25), also result in temperature-dependent sterility. P granules appear to dock with nuclear pores and are thought to be processing centers for germline transcripts (26). Thus, it seems likely that P granules function broadly to organize posttranscriptional regulation (and perhaps aspects of transcriptional regulation) in the germline, and that at least some of these regulatory mechanisms are inherently sensitive to temperature.

Adaptation to Temperature and Small-RNA Pathways. AGO systems appear to have independently evolved genome-scale regulatory capacities in diverse organisms. For example, the AGO-mediated micro-RNA (miRNA) systems of plants and animals appear to have independent evolutionary origins, and yet in both systems miRNAs have acquired hundreds of targets, many with subtle affects on gene expression (27, 28). The ALG-3/4 system provides another example of an independently evolved AGO system that has acquired hundreds of targets. The modularity of AGO/small-RNA-mediated targeting permits a single class of AGO protein to interact with hundreds or thousands of different small RNA cofactors, each of which can in turn regulate the expression of multiple targets. Consequently, the expression and sequence of

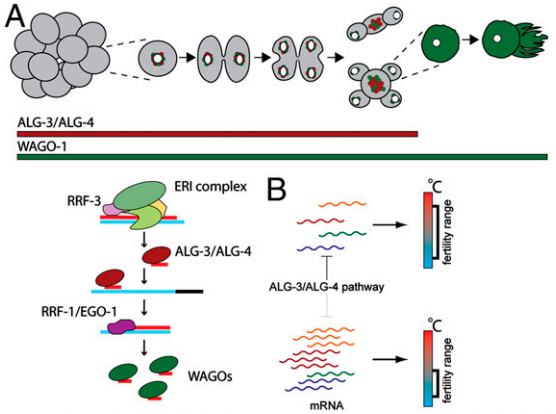

Fig. 6. Model of ALG-3/4 and WAGO-1 expression during sperm development. (*A*) Depiction of spermatogenesis and spermiogenesis, with ALG-3/4 and WAGO-1 expression indicated by the red and green bars (respectively), as well as a model for the biogenesis of 26G and 22G RNAs. The schematic in *B* illustrates a potential role for ALG-3/4 in lowering target-mRNA levels to increase robustness to temperature.

the AGO itself, as well as the expression and sequence of each specificity-determining small-RNA, can evolve independently. We hypothesize that these features provide AGO systems with the capacity to evolve rapidly, giving them the ability to superimpose new regulation on existing gene-expression networks.

The rules that govern the recognition of a transcript and trigger the biogenesis of 26G-RNAs are not yet known. The structure or expression of the target gene or transcript may promote recognition. Alternatively, all transcripts might be sampled stochastically during nuclear export and processing in the P granule, as discussed above. Whatever the mechanism for initial targeting, the presence of 22G-RNAs in mature sperm could drive a feed-forward mechanism that reinforces the recognition and silencing of ALG-3/4 targets in the next generation. Thus the ALG-3/4 system may function both broadly and heritably to promote robustness to temperature by functioning broadly in the regulation of a multitude of targets whose silencing improves the robustness of sperm to temperature.

Gametogenesis appears to be an inherently thermosensitive process both in *C. elegans* and in other metazoans. In most mammals, core body temperatures are lethal to sperm, and external male gametogenesis appears likely to represent an adaptation that was basal to the evolution of endothermy in the vertebrate lineage (29). Understanding how the *alg*-3/4 pathway promotes thermotolerant sperm development is likely to uncover general principals of gene regulation important for fertility, development, and germline maintenance in diverse organisms.

Experimental Procedures

Worm Strains and Genetics. *C. elegans* culture and genetics were as described in ref. 30. The Bristol N2 strain was used as the standard wild-type strain. Alleles used, listed by chromosome, include: Unmapped: neIs23[unc-119(+) GFP::ALG-3]; LGII: neSi1[cb-unc-119(+) GFP::WAGO-1]; LGIII: alg-4(ok1041), alg-4(1184), unc-119(ed3); LGIV: alg-3(tm1155), fem-(q20); LGV: fog-2(q71), ergo-1(tm1860).

The GFP::ALG-3 transgenic strain was generated by biolistic transformation (31). *GFP::wago-1* single-copy insertions were obtained by Mos-mediated single copy insertion (32). Details, including the generation of fusion constructs, are provided in *SI Experimental Procedures*.

Brood size analysis was performed as described (6). Males were enriched from *fog-2* or *alg-3/4;fog-2* cultures as described (33). Spermatid activation was performed as described (19). Spermatid numbers were determined by imaging male worms stained with DAPI. Additional details are provided in *SI Experimental Procedures*. Microscopy was performed as described (5).

Molecular Biology. Enrichment of small RNA and Northern blot analysis were performed as described (9). Probe sequences are provided in *SI Experimental Procedures*. Small RNAs extracted from isolated sperm, *fog-2* males and *alg-3/4;fog-2* males were pretreated with Tobacco Acid Pyrophosphatase (Epicenter Biotechnologies) and cloned using a 5′ ligation-dependent protocol (9). cDNA libraries were sequenced by the University of Massachusetts Deep Sequencing Core using an Illumina GAII. RT-qPCR was performed as described in ref. 6. Primer sequences are available upon request. Analyses of deep-sequencing and tiling array data were performed as described (9).

Accession Numbers. All RNA sequences extracted from Illumina reads and Microarray data as described were deposited in the National Center for Biotechnology Information's Gene Expression Omnibus and are accessible through Gene Expression Omnibus SuperSeries accession number GSE18731.

ACKNOWLEDGMENTS. We thank members of the Mello laboratory for helpful discussion: Darryl Conte, Jr., and Elaine Youngman for comments on the manuscript; E. Kittler and the University of Massachusetts Deep Sequencing Core facility for processing Illumina samples; P. Furcinitti and the University of Massachusetts Light Microscopy core for use of the confocal microscope; The *Caenorhabditis* Genetics Center and the laboratory of James Priess for providing strains. This work was supported in part by Predoctoral Fellowships SFRH/BD/11803/2003 (to P.J.B.) and SFRH/BD/17629/2004/H6BM (to D.A.C.) from Fundação para Ciência e Tecnologia, Portugal and by Grant R01 GM58800 from the National Institute of General Medical Sciences (to C. C.M.). J.M.C. was a Howard Hughes Medical Institute fellow of the Life Sciences Research Foundation. C.C.M. is a Howard Hughes Medical Institute Investigator.

1. Hutvagner G, Simard MJ (2008) Argonaute proteins: key players in RNA silencing. *Nat Rev Mol Cell Biol* 9:22–32.
2. Tolia NH, Joshua-Tor L (2007) Slicer and the argonautes. *Nat Chem Biol* 3:36–43.
3. Yigit E, et al. (2006) Analysis of the *C. elegans* Argonaute family reveals that distinct Argonautes act sequentially during RNAi. *Cell* 127:747–757.
4. Grishok A, et al. (2001) Genes and mechanisms related to RNA interference regulate expression of the small temporal RNAs that control *C. elegans* developmental timing. *Cell* 106:23–34.
5. Claycomb JM, et al. (2009) The Argonaute CSR-1 and its 22G-RNA cofactors are required for holocentric chromosome segregation. *Cell* 139:123–134.
6. Batista PJ, et al. (2008) PRG-1 and 21U-RNAs interact to form the piRNA complex required for fertility in *C. elegans*. *Mol Cell* 31:67–78.
7. Das PP, et al. (2008) Piwi and piRNAs act upstream of an endogenous siRNA pathway to suppress Tc3 transposon mobility in the *Caenorhabditis elegans* germline. *Mol Cell* 31:79–90.
8. Wang G, Reinke V (2008) A *C. elegans* Piwi, PRG-1, regulates 21U-RNAs during spermatogenesis. *Curr Biol* 18:861–867.
9. Gu W, et al. (2009) Distinct argonaute-mediated 22G-RNA pathways direct genome surveillance in the *C. elegans* germline. *Mol Cell* 36:231–244.
10. Ruby JG, et al. (2006) Large-scale sequencing reveals 21U-RNAs and additional microRNAs and endogenous siRNAs in *C. elegans*. *Cell* 127:1193–1207.
11. Duchaine TF, et al. (2006) Functional proteomics reveals the biochemical niche of *C. elegans* DCR-1 in multiple small-RNA-mediated pathways. *Cell* 124:343–354.
12. Gent JI, et al. (2009) A *Caenorhabditis elegans* RNA-directed RNA polymerase in sperm development and endogenous RNA interference. *Genetics* 183:1297–1314.
13. Pavelec DM, Lachowiec J, Duchaine TF, Smith HE, Kennedy S (2009) Requirement for ERI/DICER complex in endogenous RNAi and sperm development in *Caenorhabditis elegans*. *Genetics* 183:1283–1295.
14. Vasale JJ, et al. (2010) Sequential rounds of RNA-dependent RNA transcription drive endogenous small RNA biogenesis in the ERGO-1 argonaute pathway. *Proc Natl Acad Sci USA*.
15. Schedl T, Kimble J (1988) *fog-2*, a germ-line-specific sex determination gene required for hermaphrodite spermatogenesis in *Caenorhabditis elegans*. *Genetics* 119:43–61.
16. Ward S, Miwa J (1978) Characterization of temperature-sensitive, fertilization-defective mutants of the nematode *Caenorhabditis elegans*. *Genetics* 88:285–303.
17. Shakes DC, et al. (2009) Spermatogenesis-specific features of the meiotic program in *Caenorhabditis elegans*. *PLoS Genet* 5:e1000611.
18. Kawasaki I, et al. (1998) PGL-1, a predicted RNA-binding component of germ granules, is essential for fertility in *C. elegans*. *Cell* 94:635–645.
19. Shakes DC, Ward S (1989) Initiation of spermiogenesis in *C. elegans*: a pharmacological and genetic analysis. *Dev Biol* 134:189–200.
20. L'Hernault SW (2006) Spermatogenesis. *WormBook* 20:1–14.
21. Reinke V, Gil IS, Ward S, Kazmer K (2004) Genome-wide germline-enriched and sex-biased expression profiles in *Caenorhabditis elegans*. *Development* 131:311–323.
22. Aravin AA, Hannon GJ, Brennecke J (2007) The Piwi-piRNA pathway provides an adaptive defense in the transposon arms race. *Science* 318:761–764.
23. Han T, et al. (2009) 26G endo-siRNAs regulate spermatogenic and zygotic gene expression in *Caenorhabditis elegans*. *Proc Natl Acad Sci USA* 106:18674–18679.
24. Altun ZF, Herndon LA, Crocker C, Lints R, Hall DH (eds) 2002-2009. http://www.wormatlas.org.
25. Kuznicki KA, et al. (2000) Combinatorial RNA interference indicates GLH-4 can compensate for GLH-1; these two P granule components are critical for fertility in *C. elegans*. *Development* 127:2907–2916.
26. Anderson P, Kedersha N (2009) RNA granules: post-transcriptional and epigenetic modulators of gene expression. *Nat Rev Mol Cell Biol* 10:430–436.
27. Bartel DP (2004) MicroRNAs: genomics, biogenesis, mechanism, and function. *Cell* 116:281–297.
28. Bushati N, Cohen SM (2007) microRNA functions. *Annu Rev Cell Dev Biol* 23:175–205.
29. Werdelin L, Nilsonne A (1999) The evolution of the scrotum and testicular descent in mammals: a phylogenetic view. *J Theor Biol* 196:61–72.
30. Brenner S (1974) The genetics of *Caenorhabditis elegans*. *Genetics* 77:71–94.
31. Praitis V, Casey E, Collar D, Austin J (2001) Creation of low-copy integrated transgenic lines in *Caenorhabditis elegans*. *Genetics* 157:1217–1226.
32. Frøkjaer-Jensen C, et al. (2008) Single-copy insertion of transgenes in *Caenorhabditis elegans*. *Nat Genet* 40:1375–1383.
33. Miller MA (2006) Sperm and oocyte isolation methods for biochemical and proteomic analysis. *Methods Mol Biol* 351:193–201.

Supporting Information

Conine et al. 10.1073/pnas.0911685107

SI Experimental Procedures

Strains. WM200: [*alg-3(tm1155); alg-4(ok1041)*]; WM201: [*alg-3 (tm1155); alg-* 4(ok1041); fog-2(q71)]; WM202: {unc-119(ed3); neIs23[unc-119(+) GFP::ALG-3]; alg- 3(tm1155); alg-4(ok1041)}; WM203: {unc-119(ed3); neIs23[unc-119(+) GFP::ALG-3]; *alg-3 (tm1155)*; *alg-4(ok1041)*; *fog-2(q71)*}; WM204: {unc-119(ed3); ttTi5605; neSi1[cbunc-119(+) GFP::WAGO-1] II}, RFP::PGL-1; WM191: MAGO-12 (1).

Transgenic Constructs. GFP::ALG-3 as follows: A Not1 site was engineered between the ALG-3 promoter and ORF-3′UTR using PCR, followed by Not1 digestion and ligation of the promoter and ORF-3′UTR, followed by cloning into the TOPO TA vector (Invitrogen). GFP with Not1 sites on both termini was then ligated in between the promoter and ORF after digestion. The Gateaway cloning system (Invitrogen) was then used to transfer the GFP fusion to the pCT045 destination vector. The resulting plasmids were introduced into *unc-119(ed3)* strain using biolistic transformation according to (2). Transgenic strains were identified and integrated lines were crossed into *alg- 3/4(tm1155; ok1041)* background. The GFP::WAGO-1 fusion construct (1) was transferred to the vector pCFJ151.

Spermatid numbers were determined by imaging male worms stained with DAPI. Worms were grown synchronously for 65 to 70 h at 20 °C or for 46 to 51 h at 25 °C. Worms were washed off the plate containing M9, and then incubated in 70% ethanol for 5 min, followed by three washes with PBS. Samples were then incubated with DAPI (5 μg/mL) for 5 min, and again washed three times with PBS. Finally, worms were put onto indentation slides, and DAPI-stained spermatid nuclei were counted using fluorescence microscopy.

Gonads and sperm were excised from worms in 1× sperm salts containing 2-mM levamisole and DAPI (5 ug/mL) on poly-L-lysine coated slides. Images in Figs. 2A and 5B, were acquired using Solamere Technology Group CSU10B Spinning Disk Confocal System scan head mounted on a Nikon TE-2000E2 inverted microscope with a 40× Plan/APO Oil lens and a Roper Coolsnap HQ2 camera. Metamorph, ImageJ, and Adobe Photoshop software were used to analyze the images. Z sections ranging from 0.2 to 0.3 μm were collected from live worms immobilized by 2-mM levamisole (Sigma).

Probe Sequences (Northern Blot). Probe sequences were as follows: *f36h12.4,* tcatgttgccaatgattgcaattttcgtgctacttggatc; *ssp- 16*, ttattagcattgtattcatacctatcatagaaaacc; *c40a11.10,* cggaatctcaaacttttccatcttgc; SL1, ctcaaacttgggtaattaaacc.

1. Gu W, et al. (2009) Distinct argonaute-mediated 22G-RNA pathways direct genome surveillance in the *C. elegans* germline. *Mol Cell* 36:231–244.

2. Praitis V, Casey E, Collar D, Austin J (2001) Creation of low-copy integrated transgenic lines in *Caenorhabditis elegans*. *Genetics* 157:1217–1226.

A

```
ALG-3   MSRRNATNFVDNNTLTSSGISGSGSLSPPITSRPASGQASPLSSNGSLSPP--VDDQGSV 58
ALG-4   MSRRNATSFVDNNTLTSSGISGSGSMSPPITSRPASGQASPLTSNGSLSPPQYADDQGSV 60

ALG-3   SYNSDSPRDLSPLLLSELACLNMREVVARPGLGTIGRKIPVKSNFFAVDLKNPKMVVVQY 118
ALG-4   SYNLDSPRDLSPLLLSELACLNMREVVARPGLGTIGRQIPVKSNFFAMDLKNPKMVVIQY 120

ALG-3   HVEVHHPGCRKLDKDEMRIIFWKAVSDHPNIFHNKFALAYDGAHQLYTVARLEFPDDQGS 178
ALG-4   HVEIHHPGCRKLDKDEMRIIFWKAVSDHPNIFHNKFALAYDGAHQLYTVARLEFPDDQGS 180

ALG-3   VRLDCEATLPKDNRDRTRCAISIQNVGPVLLEMQRTRTNNLDERVLTPIQILDIICRQSL 238
ALG-4   VRLDCEASLPKDNRDRTRCAISIQNVGPVLLEMQRTRTNNLDERVLTPIQILDIICRQSL 240

ALG-3   TCPLLKNSANFYTWKSSCYRIPTAAGQALDLEGGKEMWTGFFSSAHIASNYRPLLNIDVA 298
ALG-4   TCPLLKNSANFYTWKSSCYRIPTAAGQALDLEGGKEMWTGFFSSAHIASNYRPLLNIDVA 300

ALG-3   HTAFYKTRITVLQFMCDVLNERTSKPNRNNPRGPGAPGG---YRGGRGGARGGSYQNFGN 355
ALG-4   HTAFYKTRITVLQFMCDVLNERTSKPNRNNPRGPGGPGGPGGYRGGRGGGRGGSYGNFGN 360

ALG-3   RGPPGANVRDDFGGNGLTFTMDTLSRDTQLSSFETRIFGDSIRGMKIRATHRPNAIRVYK 415
ALG-4   RGPPGANVRDDFGGNGLTFTMDTLSRDTQLSSFETRIFGDAIRGMKIRAAHRPNAIRVYK 420

ALG-3   VNSLQLPADKLMFQGIDEEGRQVVCSVADYFSEKYGPLKYPKLPCLHVGPPTRNIFLPME 475
ALG-4   VNSLQLPADKLMFQGIDEEGRQVVCSVADYFSEKYGPLKYPKLPCLHVGPPTRNIFLPME 480

ALG-3   HCLIDSPQKYNKKMTEKQTSAIIKAAAVDATQREDRIKQLAAQASFGTDPFLKEFGVAVS 535
ALG-4   HCLIDSPQKYNKKMSEKQTSAIIKAAAVDATQREDRIKQLAAQASFGTDPFLKEFGVAVS 540

ALG-3   SQMIETSARVIQPPPIMFGGNNRSINPVVFPKDGSWSMDHQTLYMPATCRSYSMIALVDP 595
ALG-4   SQMIQTTARVIQPPPIMFGGNNRSVNPVVFPKDGSWTMDNQTLYMPATCRSYSMIALVDP 600

ALG-3   RDQTSLQTFCQSLTMKATAMGMNFPRWPDLVKYGRSKEDVCTLFTEIADEYRVTNTVCDC 655
ALG-4   RDQTSLQTFCQSLTMKATAMGMNFPRWPDLVKYGRSKEDVCTLFTEIADEYRVTNTVCDC 660

ALG-3   IIVVLQSKNSDIYMTVKEQSDIVHGIMSQCVLMKNVSRPTPATCANIILKLNMKMGGINS 715
ALG-4   IIVVLQSKNSDIYMTVKEQSDIVHGIMSQCVLMKNVSRPTPATCANIVLKLNMKMGGINS 720

ALG-3   RIVADQITNKYLVDQPTMVVGIDVTHPTQAEMRMNMPSVAAIVANVDLLPQSYGANVKVQ 775
ALG-4   RIVADKITNKYLVDQPTMVVGIDVTHPTQAEMRMNMPSVAAIVANVDLLPQSYGANVKVQ 780

ALG-3   KKCRESVVYLLDAIRERIITFYRHTKQKPARIIVYRDGVSEGQFSEVLREEIQSIRTACL 835
ALG-4   KKCRESVVYLLDAIRERIITFYRHTKQKPARIIVYRDGVSEGQFSEVLREEIQSIRTACL 840

ALG-3   AIAEDFRPPITYIVVQKRHHARIFCKFPNDMVGKAKNVPPGTTVDTGIVSPEGFDFYLCS 895
ALG-4   AIAEDFRPPITYIVVQKRHHARIFCKYQNDMVGKAKNVPPGTTVDTGIVSPEGFDFYLCS 900

ALG-3   HYGVQGTSRPARYHVLLDECKFTADEIQNITYGMCHTYGRCTRSVSIPTPVYYADLVATR 955
ALG-4   HYGVQGTSRPARYHVLLDECKFTADEIQSITYGMCHTYGRCTRSVSIPTPVYYADLVATR 960

ALG-3   ARCHIKRKLGLADNNDCDTNSLSSSLASLLNVRTGSGKGKKSHAPSVDDESYSLPDAASD 1015
ALG-4   ARCHVKRKLGLADNNDCDTNSRSSTLASLLNVRTGSGKGKKSYAPSVDDESYSLSDATSD 1020

ALG-3   QILQDCVSVAADFKSRMYFI                                          1035
ALG-4   QILQDCVSVATDFKSRMYFI                                          1040
```

B

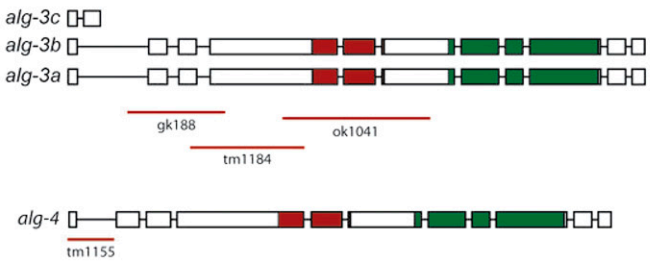

Fig. S1. Amino acid alignment and gene models for *alg-3 and alg-4.* (*A*) Alignment of amino acid sequences for *alg-3* and *alg-4* using clustalW2. (*B*) Gene models for *alg-3* and *alg-4*.

	Shift	L2/L3	L3/L4	L4/YA	GA
embryo hatched at 25°C	to 20°C	++	++	+	-
embryo hatched at 20°C	to 25°C	-	-	+	+

++ average progeny similar to worms maintained at 20°C;
+ average progeny <50% of worms maintained at 20°C;
- no progeny

Fig. S2. The temperature-sensitive period for alg-3/4 double mutants. Worms were hatched at either 20 °C or 25 °C and then shifted to the opposite temperature at the indicated larval stage and the brood size was determined.

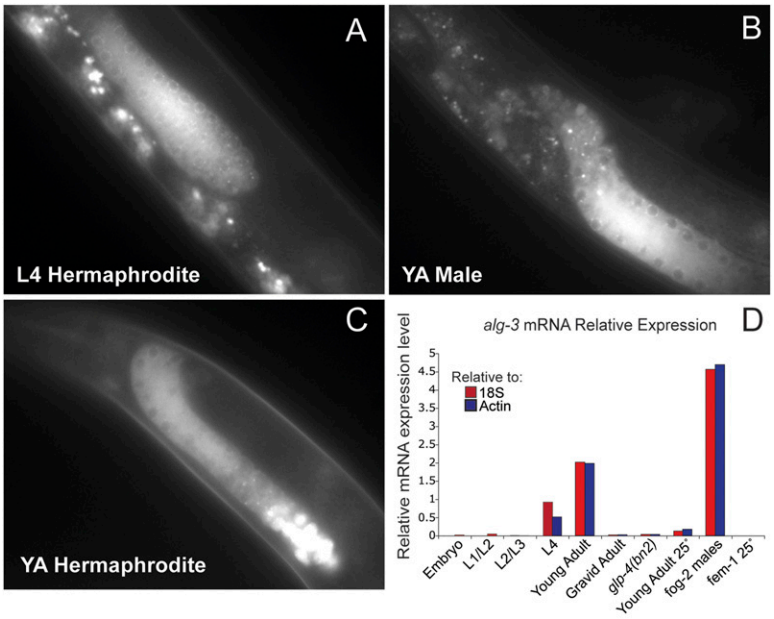

Fig. S3. ALG-3 is expressed during spermatogenesis. (*A*–*C*) Fluorescence microscopy of GFP::ALG-3 in a wild-type L4 hermaphrodite and in young adult (YA Male and Hermaphrodite) animals, as indicated. (*D*) Quantitative real-time PCR analysis of *alg-3* mRNA expression using *actin* mRNA (blue bars) or 18s rRNA (red bars) as a normalization standard.

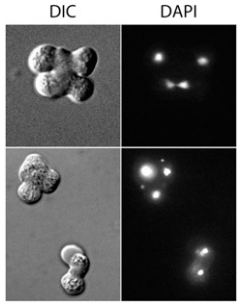

Fig. S4. *alg-3/4* mutant defects in spermatogenesis. DIC and DAPI images of *alg-3/4* developing spermatocytes with defects in DNA intergrity and budding from the residual body.

Fig. S5. 26G-RNA distribution on targets. *f59a6.2* exhibits *5′* bias, *eft-3* exhibits 3′ bias, and *ssp-16* exhibits no bias. Arrows represent 1 to 3 reads (cyan), 3 to 10 reads (violet), and greater than 10 reads (red). To emphasize this bias, the number of reads in some cases are labeled.

Other Supporting Information Files

Table S1 (DOC)
Table S2 (DOC)
Table S3 (DOC)
Table S4 (DOC)
Table S5 (DOC)